

Article

Investigation on Synaptic Adaptation and Fatigue in ZnO/HfZrO-Based Memristors under Continuous Electrical Pulse Stimulation

Zeyang Xiang, Kexiang Wang, Jie Lu, Zixuan Wang, Huilin Jin, Ranping Li, Mengrui Shi, Liuxuan Wu, Fuyu Yan and Ran Jiang *

Faculty of Electrical Engineering and Computer Science, Ningbo University, Ningbo 315211, China

* Correspondence: jiangran@nbu.edu.cn

Abstract: This study investigates the behavior of memristive devices characterized by oxygen-deficient ZnO and HfZrO films under continuous pulse stimulation. This dynamic reflects the adaptability observed in neural synapses when repeatedly subjected to stress, ultimately resulting in a mitigated response to pressure. Observations show that the conductivity of memristors increases with the augmentation of continuous electrical pulses. However, the momentum of this growth trend gradually diminishes, highlighting the devices' capability to adapt to repetitive pressure. This adjustment correlates with the transition of biological synapses from short-term to persistent memory stages, aligning with the principles of the Ebbinghaus memory model. The architecture of memristors, integrating ZnO and HfZrO in a layered manner, holds promising prospects in replicating the inherent synaptic features found in biological organisms.

Keywords: memristor; synaptic behavior; polarization; electrical stimulation



Citation: Xiang, Z.; Wang, K.; Lu, J.; Wang, Z.; Jin, H.; Li, R.; Shi, M.; Wu, L.; Yan, F.; Jiang, R. Investigation on Synaptic Adaptation and Fatigue in ZnO/HfZrO-Based Memristors under Continuous Electrical Pulse Stimulation. *Electronics* **2024**, *13*, 1148. <https://doi.org/10.3390/electronics13061148>

Academic Editor: Francesco Driussi

Received: 18 February 2024

Revised: 7 March 2024

Accepted: 12 March 2024

Published: 21 March 2024



Copyright: © 2024 by the authors. Licensee MDPI, Basel, Switzerland. This article is an open access article distributed under the terms and conditions of the Creative Commons Attribution (CC BY) license (<https://creativecommons.org/licenses/by/4.0/>).

1. Introduction

The swift progress in neuromorphic computing draws inspiration from the human brain's remarkable capacity to process information, especially in discerning intricate environmental signals and visuals [1]. For the precise duplication of brain functionalities and the advancement of neuromorphic systems, technologies emulating synapses have become crucial [2]. Conventional von Neumann architectures, dependent on either densely packed resistor-capacitor CMOS circuits or software strategies, confront issues like excessive energy use and substantial space demands [3]. As a result, the focus is increasingly on crafting innovative devices equipped with self-reliant synaptic functions, notably memristor-based electronic synapses, marking a fresh research trajectory. Since its initial conceptualization in 1971, the memristor has led the charge in electronic synapse research, celebrated for its conductance modulation capabilities and its proficiency in simulating synaptic weight adjustments [4].

While memristors have demonstrated notable progress in emulating synaptic behaviors, a research void exists concerning their ability to authentically replicate the adaptive fatigue or habituation responses characteristic of biological synapses as standalone units. CMOS technology has not fully captured the unique attributes of the human sensory system, which responds to stimuli with particular traits, notably in facilitating approach-avoidance reactions, capable of adaptively ignoring or highlighting potential dangers [5]. This encompasses habituation (adapting to and disregarding stimuli) and sensitization (initiating alarms and bolstering reactions). In a state of habituation, stimuli are overlooked, whereas in sensitization, reactions to stimuli are intensified. Replicating these inherently natural and complex responses in inorganic devices is challenging, yet memristors hold substantial promise for future device and humanoid robot development. Extant research has noted

memristor responses to electrical stimuli that mirror those of biological synapses. Innovations in paired pulse facilitation (PPF) behavior have shown parallels between inorganic memristors and biological synapses in terms of their response to electrical stimuli, with the PPF mechanism being ascribed to the cumulative effect of dual pulses on a memristor [6,7].

The Paired Pulse Facilitation (PPF) phenomenon demonstrated the resemblance between memristors and synaptic responses. Li and colleagues documented the PPF phenomenon on $\text{CeO}_2/\text{Nb-SrTiO}_3$ memristors [8]. PPF can also be detected in memristor-based systems such as La:HfO_2 [9], $\text{AlO}_x/\text{HfO}_x$ [10], HfSiO_x [11], and $\text{Pt/HfO}_2/\text{TaO}_x/\text{TiN}$ [12]. Recently, memristors with nanostructure underwent training using uninterrupted pulses by different groups [13,14]. Zhao et al. developed a photoelectric memristor using a zinc oxide/poly(3-hexylthiophene) heterojunction. This memristor was able to replicate the learning and forgetting cycles of the human brain through three iterations [15]. In addition, p+-Si/n-ZnO heterojunctions [16], ferroelectric second-order based on $\text{Pt/BiFeO}_3/\text{SrRuO}_3$ [17], and p-NiO/n-ZnO heterojunction memristors [18] have the ability to replicate the experiential learning process of the biological brain. Nevertheless, natural biological neural responses exhibit both immediate and simultaneous non-associative learning. Non-associative learning plays a vital role in how organisms react to stimuli in the field of biology. Zhao et al., have conducted studies on simulating non-associative learning using zinc oxide nanowire memristors. The memristor displayed distinct behaviors in both positive and negative directions. Hong et al. developed a memory circuit specifically for non-associative learning [19]. Sun et al. developed a memristor circuit that enables non-associative learning in various emotional states [20]. In light of the current situation, where achieving different response behaviors in non-associative learning necessitates artificially altering the voltage polarity in both directions, and the requirement for memory circuits designed for non-associative learning, we suggest employing straightforward bilayer polarized self-regulating devices to accomplish habituation or sensitization monitoring using a unidirectional voltage. Nonetheless, under continuous stimulation, it remains uncertain if memristors display a uniform increase akin to PPF (limited to a pair of pulses) measurements. Moreover, the frequent reporting that an accumulation of electrical stimuli may facilitate a shift from short-term memory (STM) to long-term memory (LTM) begs the question of the relationship between such a transition and the accumulation of electrical stimulation [21,22]. This investigation utilizes ZnO/HfZrO stacked structures for crafting memristors, taking advantage of the well-established ferroelectric properties of HfZrO, which are influenced by the concentration of oxygen vacancies. Through examining habituation behavior under incessant electrical pulse stimulation, we discerned a semi-fatigue behavior closely paralleling the shift from STM to LTM [23]. The distinctive behavior of memristors under constant stimulation underscores their potential in simulating biological synapses through inorganic means.

In this study, HfZrO and ZnO were chosen as the primary materials for constructing memristors, based on their unique physical and chemical properties, which are crucial for optimizing the performance of memristors. HfZrO was selected for its pronounced ferroelectric properties [24], which exhibit stability at the nanoscale, playing a decisive role in simulating the short-term to long-term memory transition (STP to LTP transition) in biological synapses. The ferroelectric HfZrO films demonstrate stable high remanent polarization and reversible polarization direction switching [25], which we believe to be the main reason for the fatigue phenomenon described in our study, as devices without ferroelectric properties did not exhibit similar fatigue phenomena. ZnO, being an n-type semiconductor with a wide bandgap and high electron mobility, makes it an ideal material for controlling and tuning the conductance window, thereby optimizing the synaptic simulation performance. Numerous studies have reported ZnO's excellent resistive switching and memristive hysteresis characteristics [26]. The combination of HfZrO and ZnO not only leverages their respective advantages, but also optimizes the response time and synaptic efficiency by facilitating effective migration and distribution of charge carriers between electrodes. This synergistic effect of the layered materials not only enhances

the adaptability of device to continuous electrical pulse stimulation but also improves its performance in simulating biological synaptic behavior, particularly observed in the fatigue and adaptability exhibited in our research. Specifically, the combination of the ferroelectric properties of the HfZrO layer with the conductive capabilities of the ZnO layer allows for fine control of current and conductance under different stimulation conditions by adjusting the distribution and concentration of oxygen vacancies, thereby simulating the transition from short-term to long-term memory in biological synapses.

Since the discovery of the PPF effect, there has been a lot of interest in synaptic research, with a lot of work being done on single-device synaptic simulations. For example, some studies have used In-Ga-Zn-O (IGZO) thin-film devices as synaptic elements in neural networks, resulting in cellular neural networks capable of learning simple logic functions [27]. Other research has looked into the development of bidirectional gradual switching capabilities in synaptic cross arrays to mimic the long-term potentiation/inhibition properties of biological synapses [28]. In previous research, one can discover that memristors could be artificially designed to achieve synaptic biomimicry, either using hardware-designed cross array structures or software-based neural network algorithms. However, the neural responses of natural biological entities are intrinsic, natural, and concurrent. Whether the synaptic response is achieved through hardware or software design, it does not come as close to an entity's natural response to stimuli as the original research intention. The interesting habituation and adaptability behaviors were discovered based on the inherent properties of the material composition, similar to the biological tendency to move toward favorable environments and away from harmful ones, opening up new research avenues. This phenomenon of adaptability to stimuli demonstrated by devices that combine ferroelectric and memristive thin films. The ferroelectric and n type memristor structure shows great potential in mimicking the synapse. Meanwhile, this study employs high-frequency stimulation, and future research will use mixed high-frequency stimulation to mimic environmental information stimuli, indicating a new approach in our work. We used 1 V pulse stimulation (which was typically higher in previous studies) due to the high stimulation frequency and device tolerance. At lower voltage stimulation, the device remained stable and reliable. Changing the stimulation frequency on a regular basis, however, can have an impact on device performance. This topic is currently being researched.

2. Experimental

The fabrication process is outlined as follows: Initially, a layer of Al, 200 nm in thickness, was thermally evaporated onto a SiO₂/Si substrate. Subsequently, a HfZrO film, 50 nm thick, was sputtered onto the Al/SiO₂/Si base using RF magnetron sputtering in an Ar/O₂ mix, employing a Hf/Zr composite target. The oxygen partial pressure was meticulously set to 8×10^{-5} torr, with an Ar partial pressure of 2×10^{-3} torr, a ratio proven to yield oxygen-deficient oxides via RF sputtering. The sputtering was powered at 200 W. Following this, a ZnO film, also 50 nm thick, was deposited on the HfZrO layer, this time in an Ar/O₂ atmosphere using a Zn target, adjusting the oxygen partial pressure to 3.4×10^{-4} torr and maintaining the Ar at 2×10^{-3} torr to achieve the optimal ZnO composition. The device's top electrode, comprising a 100 nm Au/20 nm Ti layer, was then applied at room temperature through electron beam evaporation. Electrical assessments of the synaptic memristor were conducted at ambient temperature using the Keithley 4200 system, incorporating a high-frequency module among others, and included tests at varying temperatures. Both programming and reading operations were executed in pulse mode, with current directed from the top to the bottom electrode considered as positive bias.

Figure 1 illustrates the structural illustration of the memristor alongside its parallel to neural synapses. In Figure 1a, the configuration of ZnO and HfZrO films beneath an Au/Ti top electrode and an Al bottom electrode is depicted. This arrangement mirrors the function of a neural synapse, with oxygen vacancies serving the role of neurotransmitters, thereby influencing the device's conductance, analogous to synaptic weight. Diagram

(b) depicts the transit of neurotransmitters within synapses, akin to the movement of oxygen vacancies within the memristor. The Atomic Force Microscopy (AFM) image (c) presents the surface of the ZnO layer, and the Scanning Electron Microscopy (SEM) cross-sectional view (d) reveals a distinct demarcation between the ZnO and HfZrO films. The homogeneity observed in the AFM snapshot reflects meticulous deposition control, while the SEM cross-section evidences precise stratification, indicative of superior interface integrity and film consistency—key aspects for the dependability and efficiency of the device. The enhanced synaptic behavior exhibited by the memristor device is directly correlated with the clarity of the interface and the uniformity of the layers captured in the SEM image. The device's stable and repeatable switching characteristics, which are essential for the reliable performance of memristive applications, are supported by the uniformity in layer thickness and the absence of interfacial diffusion or intermixing.

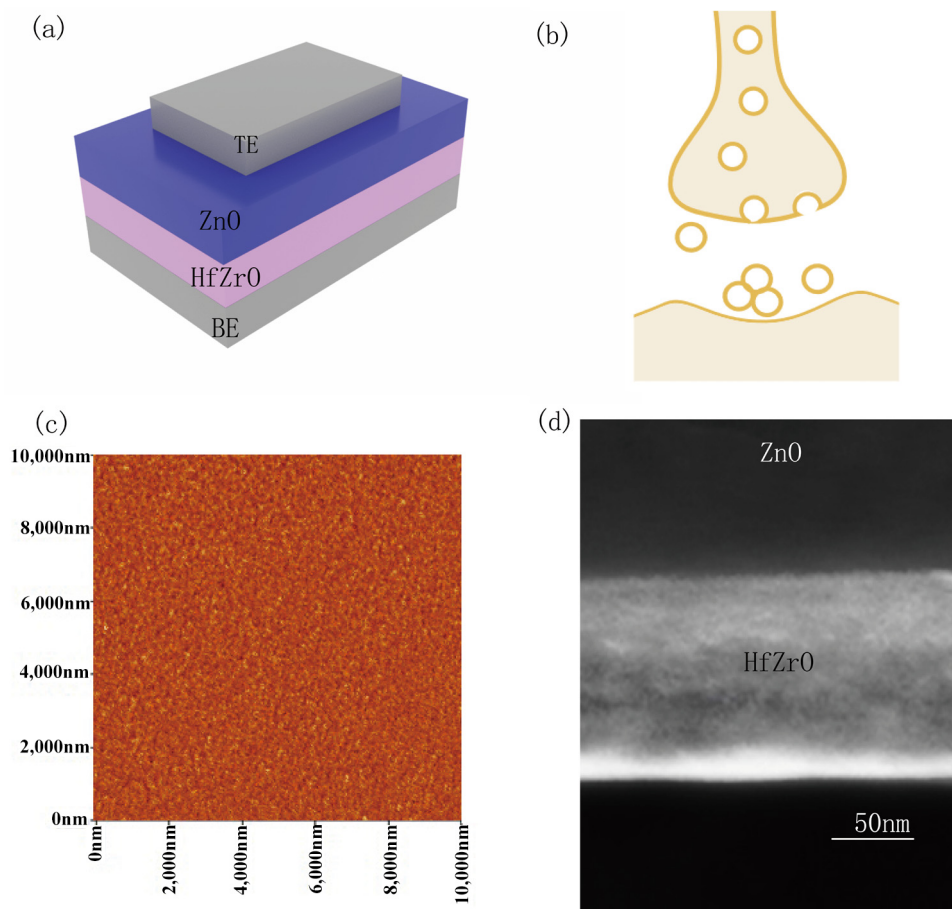


Figure 1. Fundamental characteristics of the prepared samples for synaptic memristors based on ZnO/HfZrO. (a) Device structure with a top electrode (Au/Ti layers) and a bottom electrode (Al layer) interfacing with ZnO and HfZrO layers, respectively. (b) Biological synapses with neurotransmitters in the synaptic gap. (c) Surface morphology through AFM imaging. (d) SEM cross-section of ZnO and HfZrO.

3. Results and Discussion

As shown in Figure 2a, continuous pulses with fixed intensity and width are applied to the memristor. The post-synaptic current triggered by subsequent pulses is greater than the current generated by preceding pulses, akin to the paired-pulse facilitation (PPF) behavior observed in biological synapses. PPF represents synaptic plasticity, where a second neural pulse, following closely after the first, amplifies the post-synaptic response. Upon deactivating the voltage, the post-synaptic current does not vanish instantly. Instead, a decay in the post-synaptic current is observed during the off period of the pulse, resembling

memory loss in biological systems. It is well known that PPF is associated with incomplete compensation of oxygen vacancies [29–31]. After the first pulse, oxygen vacancies can be compensated for by oxygen, and if the pulse interval is small enough, the oxygen vacancies will not be fully compensated, thus the conductive channel does not completely disappear, resulting in a higher post-synaptic current after the second pulse [29,32]. This PPF behavior, stimulated by a pair of pulses, provides a avenue to investigate the post-synaptic current as a function of pulse number in memristor synapses.

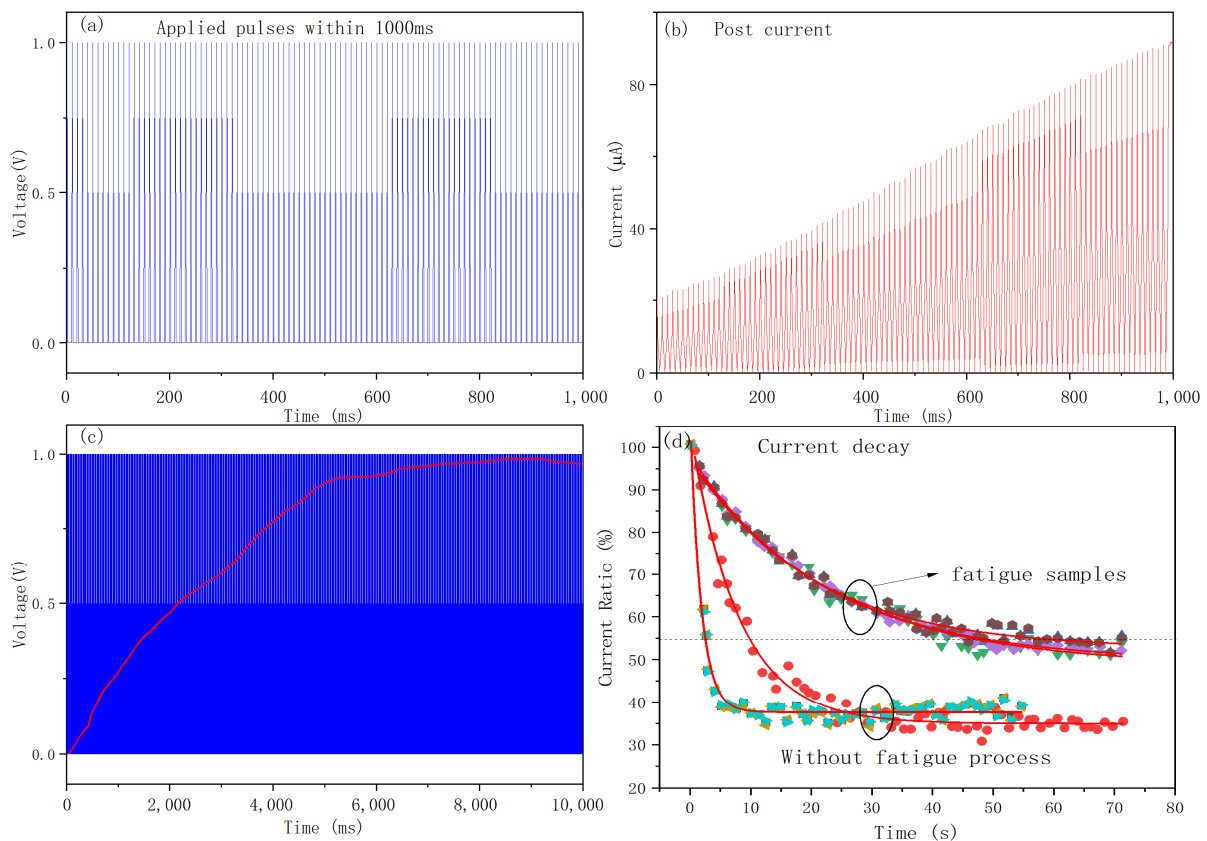


Figure 2. (a) Pulses applied within 1000 ms, with a pulse width of 20 ms, an interval of 100 ms, and an amplitude of 1 V. (b) Post-synaptic current response of the device to the pulse train. On one hand, continuous application of voltage leads to a continuous increase in device conductivity; on the other hand, the magnitude of this increase gradually diminishes. (c) Pulses applied within 10,000 ms, with a pulse width of 20 ms, an interval of 100 ms, and an amplitude of 1 V. The red line represents the corresponding peak line of the post-synaptic current response. It is evident that the later current is higher than the earlier current, but with a slower rate of increase. (d) Current decay after different numbers of pulse stimuli. For samples reaching the fatigue region, the current decay rate is almost the same. For devices that did not reach fatigue due to insufficient pulse training, the current decay curves for different pulse counts are different, with faster decay rates and lower retention values.

As shown in Figure 2b, with the application of continuous voltage, the device's conductivity continues to increase. An interesting phenomenon is that the magnitude of current increase gradually diminishes with an increase in the number of pulses. In other words, although the stimulation still leads to subsequent current being greater than the preceding one, the magnitude of increase gradually decreases, akin to the habituation or fatigue response of the brain to repetitive stimuli. If regular stimuli are deemed safe, this habituation or fatigue response parallels the acceptance and adjustment seen in biological approach-avoidance behaviors [33], which suggest the foundation for further expansion studies. The behavior of the ZnO-HfZrO device under a series of high-frequency pulse stimulations (10,000) is shown in Figure 2c. The red curve in the inset represents the

peak line of the post-synaptic current response. It is evident that the later current is higher than the earlier current, but with a characteristic of slower rate of increase (as the pulse number increases, the increase in current for each pulse gradually decreases). Once reaching a certain number, the current remains almost constant (here, it is approximately considered saturated and unchanged after more than 5500 pulse stimulations). The analysis of the current decay under various pulse stimulations revealed a memory fading-like phenomenon, where the duration for memory fade extends with the pulse count, shifting from a span of seconds to tens of seconds, and the retention percentage climbs from an estimated 37% to around 64%. This trend signifies a diminishing rate of memory loss alongside a consistent accrual of retained data. In the realm of psychology, memory dynamics are segmented into short-term memory (STM) and long-term memory (LTM), distinguished by their retention durations [34,35]. Mirroring the biological brain's rehearsal mechanism, the shift from STM to LTM can be facilitated by repeated pulse stimulations. This investigation illustrates that the memristor's exhibited fatigue from such repetitive stimulations markedly aligns with the transition from STM to LTM, as depicted in Figure 2d, where the current trajectory within the fatigue domain largely remains stable. Conversely, absent fatigue, illustrated by the curves in Figure 2d where the pulse stimulation fails to propel the memristor into the "fatigue" zone, showcases a pronounced rapid current decay phase. The distinct demarcation seen in the current trajectories of Figure 2d aligns with the device's adaptation to or fatigue from adequate stimulation. Defining STM and LTM biologically is complex [23]; however, they are generally recognized as either temporary (lasting minutes or less) or permanent (spanning hours to years) enhancements of neural connections [36]. Moreover, STM can morph into LTM through continuous rehearsal, involving structural modifications within neurons. Our device demonstrates a similar pattern, showcasing memory retention durations that align with this definition [37].

For devices not yet in the "fatigue zone," current retention at about 55% persists for under 20 s. Conversely, devices experiencing fatigue maintain this level for beyond 70 s, with the potential for even longer durations as depicted in Figure 3a. This 55% benchmark was selected because it marks the point where current reaches a state of fatigue saturation. This pivotal threshold closely coincides with fatigue's emergence (around 5500 pulses, as highlighted in Figures 2c and 3a). Therefore, upon reaching the fatigue phase, a memristor exhibits a gradual and consistent rate of current decay. This characteristic, substantially unchanged despite further pulsing (illustrated in Figure 2d), might indicate a shift towards a long-term memory (LTM) phase [38].

For a detailed examination of short-term memory (STM) phenomena, an exponential decay function is applied to model the relaxation dynamics, formulated as:

$$R(t) = R_s + (R_0 - R_s)\exp(-t/\tau) \quad (1)$$

$R(t)$ signifies the level of current retention at any given moment t , R_0 the initial retention level, and R_s the saturation level of current retention showcased in Figure 2d. The variable τ , the relaxation time, serves to quantify memristor forgetfulness. The enduring level of current retention (R_s), set to remain constant for up to 72 h as shown in Figure 3a, was examined across various pulse excitation counts. This exploration revealed that habitual stimulation lessens the forgetfulness rate while enhancing the current retention ratio. The relaxation period documented in Figure 3b aligns with the saturation trend observed in current fluctuations in Figure 2c, affirming that achieving current retention saturation (or fatigue response) may signify the attainment of LTM [39]. Figure 3c outlines the decay trajectories at differing temperatures, showcasing temperature's effect on STM's relaxation mechanism. With rising temperatures, relaxation periods shorten, a correlation supported by the literature indicating a direct relationship between the current's relaxation time and the diffusion coefficient. Given the dynamic migration of oxygen vacancy, the temperature dependency of the diffusion coefficient D is described by: $D(T) \propto \exp(-E/kT)$. Here, E represents activation energy, and k the Boltzmann constant. Hence, dynamic

dispersion of oxygen vacancies is similarly modeled by the exponential decay equation, proposing that such migration could facilitate the STM to LTM transition [40].

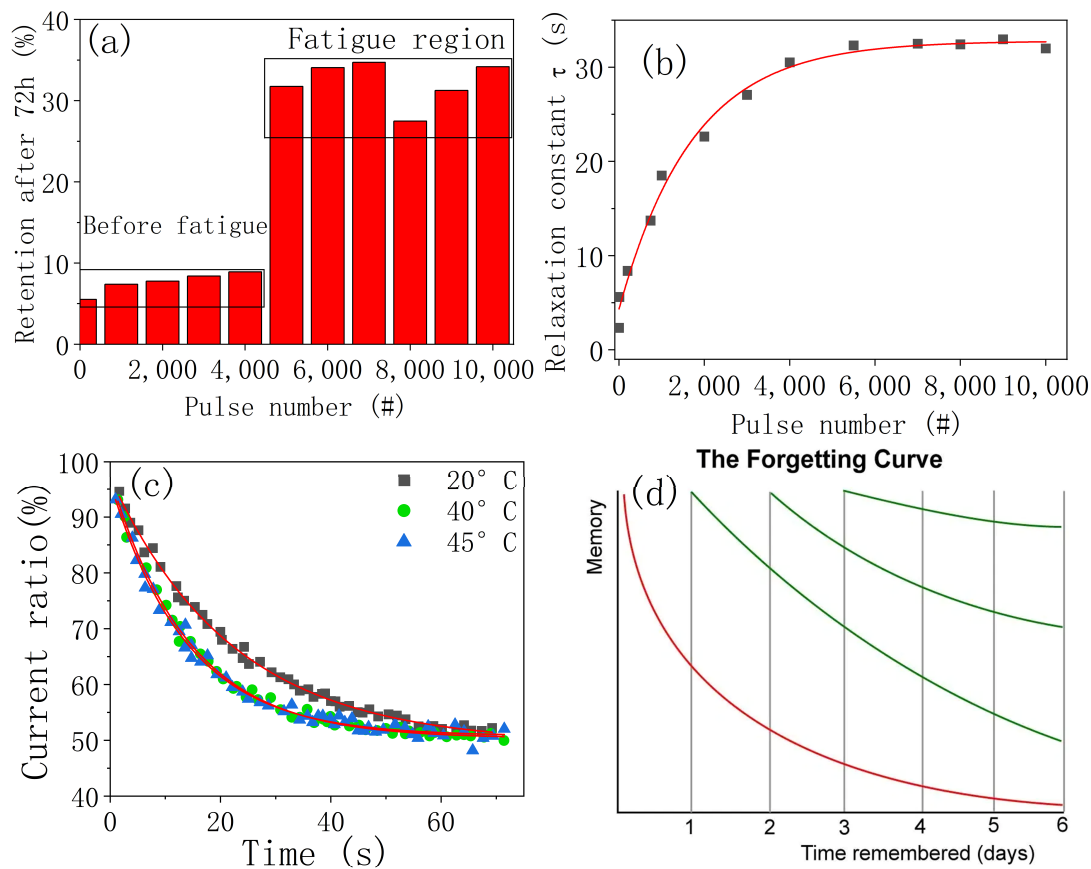


Figure 3. The impact of various parameters on fatigue effects. (a) Current retention decay of the device 72 h post-stimulation with varying numbers of pulses. The “before fatigue “and “fatigue region” were separated with gray box. # denotes the number of the pulses. (b) The relaxation time constant (τ) varies with the number of stimulation pulses, derived from fitting the data in Figure 2. Its trend highly resembles the red curve in Figure 2c. (c) Current decay of devices that reached fatigue after sufficient pulse stimulation at different temperatures. The red solid line represents the curve fitted using Equation (1). (d) The Ebbinghaus forgetting curve (sourced from the Ebbinghaus forgetting curve at <https://e-student.org/ebbinghaus-forgetting-curve/>, accessed on 29 January 2024). Red and green lines are all forgetting curves with different loss rate.

The dynamic migration of oxygen ions within the device framework is driven not merely by the applied electric field (drift), but is also significantly influenced by the concentration gradient (diffusion) [41,42]. This movement results in the modulation of the interface barrier in ZnO, which decreases or increases contingent upon the application or cessation of pulse voltage, respectively. This interface barrier is subject to transformations that arise from both the intrinsic polarization field and the external electric field, manifesting changes in both the energy height and physical width due to the dual influence of internal and external forces [43].

X-ray photoelectron spectroscopy (XPS) analyses focusing on the O 1 s spectra within ZnO films, as depicted in Figure 4a, reveal distinct differences between samples subjected to sufficient pulsing (fatigued or adapted) and those that are not, despite a fundamental similarity in the XPS spectra between fresh and insufficiently stimulated samples. Such differences may serve as robust evidence for the transition from short-term to long-term memory. It implies that the state of fatigue or adaptation is indeed brought about through changes in the oxygen bonding and composition within ZnO. Decomposition of the O

1 s peak into its components at 530.6 and 532.6 electron volts [44,45], using a Gaussian-Lorentzian blend, associates these binding energies typically with chemically bonded oxygen and oxygen that is loosely bound either on the film's surface or within interstitial voids. Notably, fresh samples exhibit a minimal presence of oxygen-deficient states (at 531.5 eV), corroborating the anticipated over-oxidation of the ZnO layer, as discussed in the experimental section. Under the influence of pulse stimulation, oxygen ions are propelled towards the surface [46]. Upon attaining a state of fatigue (with adequate pulse stimulation), it is conceivable that structural changes in the surface chemical bonds may occur, potentially culminating in the establishment of long-term memory, as illustrated in Figure 4a. A significant shift to the left in the O 1 s peak is observed, underscoring the alterations in chemical bond structures. Additionally, to confirm the lasting impact of the intrinsic polarization field, we verified the ferroelectric properties of the examined HfZrO films through P-V measurements, as depicted in Figure 4b. In our highly oxygen-deficient HfZrO films, a thickness-independent ferroelectric response is significant [47].

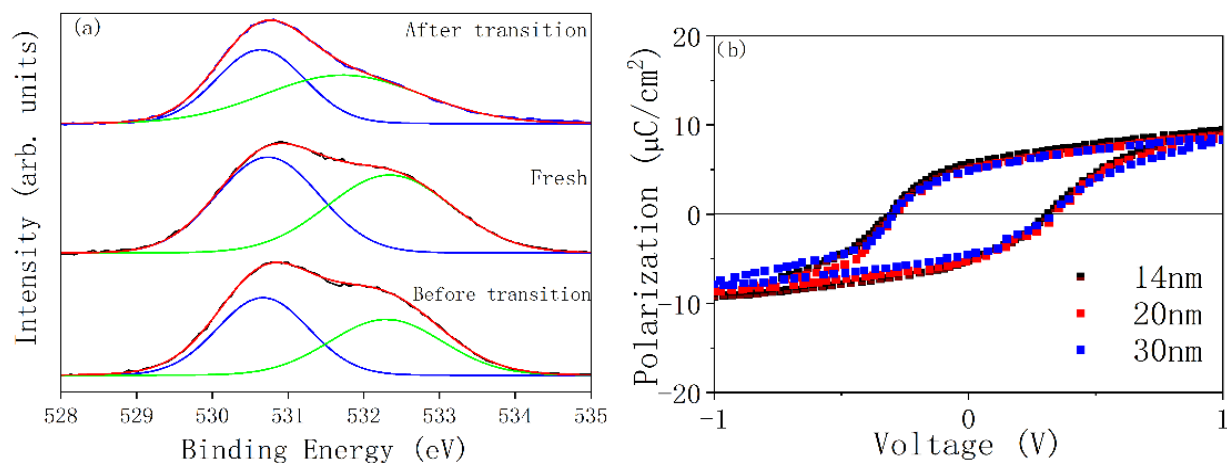


Figure 4. (a) XPS spectra of the device under various conditions. Red line represents the fitted curve, the black line represents the measured data, and the blue and green lines represent the fitted subpeaks. (b) Ferroelectric behavior of HfZrO layers with varying thicknesses.

Oxygen ion migration induces concentration gradients within the ZnO layer, alongside ferroelectrically driven ion diffusion, marking another pivotal dynamic process [48]. Analyzing oxygen vacancy movement (negatively charged oxygen ions, O^{2-}), unveils specific memory mechanisms, as illustrated in Figure 5. The electrical conductivity of ZnO is intrinsically tied to its oxygen levels, with increased oxygen correlating to diminished conductivity [49]. Applying a positive bias to the top electrode, where ZnO is more oxygen-rich, prompts the electrically induced migration of oxygen ions, condensing the high-resistance, oxygen-rich ZnO layer and thus enhancing device conductivity [50]. Concurrently, the oxygen-deficient HfZrO layer undergoes polarization. This movement of oxygen vacancies, along with ferroelectric polarization in the HfZrO layer, modulates the thickness ratio of oxygen-deficient to oxygen-rich layers, affecting device conductivity as depicted in Figure 5a,b.

Upon bias removal, expected reversion of oxygen vacancies is impeded by the inherent polarization of the oxygen-deficient HfZrO layer, leading to only a partial withdrawal of the conductive zone and a decrease in device conductivity, mirroring the current decay observed upon pulse cessation as shown in Figure 5c. Subsequent pulse application, especially with minimal intervals, results in compounded dynamic processes due to lingering polarization, expanding the conductive area and raising current, as demonstrated in Figure 5d. Frequent, high-frequency stimulation may prevent oxygen vacancy back-diffusion, potentially aiding the STM to LTM transition as HfZrO polarization becomes more entrenched. During this reverse recovery, some oxygen ions reassociate with vacancies, offsetting the localized structural alterations underlying STM. In our devices, the inherent polarization of

the HfZrO layer eases the STM to LTM shift. With enhanced pulse stabilization, we might observe a new form of non-volatile “trained memory” behavior. The synergy between HfZrO and ZnO films is critical. The extensively oxygen-deficient HfZrO film creates a ferroelectric polarized environment responsive to external voltage, while ZnO substantial oxygen content furnishes a wealth of negative charge carriers, facilitating an uptick in post-synaptic current through oxygen vacancy-based conductive pathways.

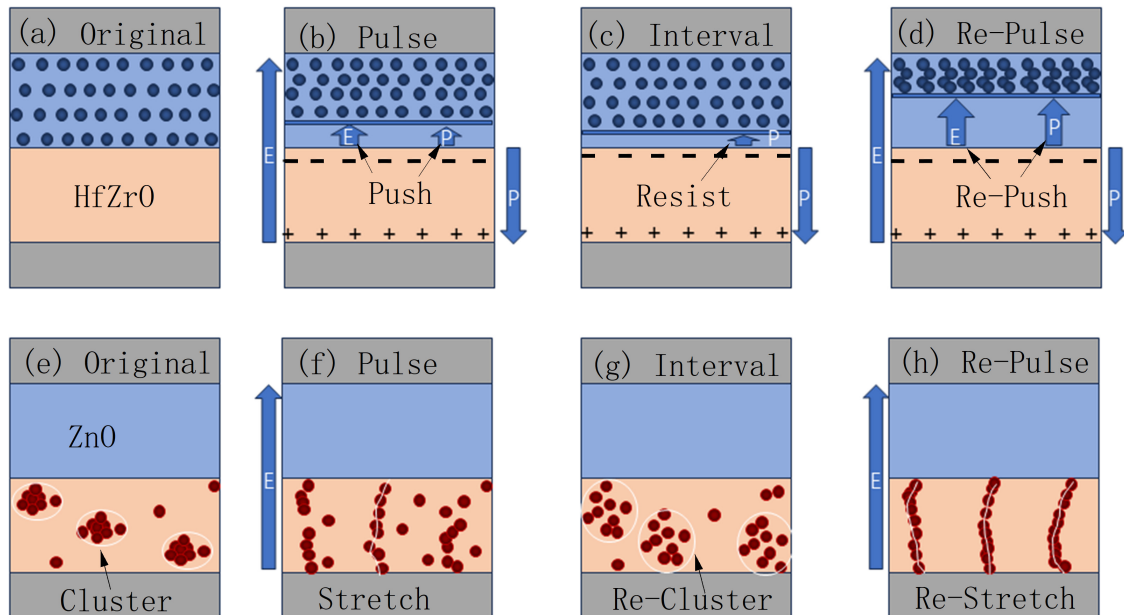


Figure 5. Dynamic processes within the device. For the ZnO layer: (a) in initial state, (b) during the pulse, (c) when the pulse ceases, and (d) during subsequent pulsing. “E” represents the external electric field, and “P” represents the polarization field. Similarly for the HfZrO layer: (e) in initial state, (f) during the pulse, (g) when the pulse ceases, and (h) during subsequent pulsing.

Our investigations [51] corroborate findings by Dr. Yang’s group [52], highlighting localized clusters within Hf/Zr oxide films, akin to silver clusters in previous research, as validated with comprehensive XPS analyses. This observation introduces another pivotal dynamic mechanism, potentially leading to Paired-Pulse Facilitation (PPF)-like current enhancements in the HfZrO layer, which is further explained alongside the depictions in Figure 5e,f. These clusters, which fluctuate between contracting in the high-resistance state (HRS) and expanding in the low-resistance state (LRS), facilitate resistance switching through the formation or disruption of connectivity between neighboring cluster locations. Silver nanoparticles and oxygen vacancies exhibit parallel behaviors to synaptic inflow and calcium ion efflux in biological cells, to a certain extent. Voltage pulse applications provoke localized thermal increments due to Joule heating and induce potential tilting by the electric field’s effect on oxygen vacancy (or charged oxygen ion) clusters, causing the disintegration of larger clusters. As clusters are redistributed more uniformly within the active layer, resistance diminishes, leading to current and temperature rises, which, through a positive feedback loop, foster the creation of conductive channels. Upon deactivation of the voltage, temperature falls and oxygen vacancies commence reversion, with most returning to cluster formations upon the voltage’s removal, thereby reinstating the high-resistance state and nearly reverting to the initial conductive path configuration, yielding volatility. Sequential pulse applications suggest a conductance evolution mirroring synaptic behaviors. The initial voltage pulse induces oxygen vacancy migration out of clusters, facilitating inter-cluster connections. Should pulse intervals remain below the oxygen vacancy restoration threshold, further conductive channels form, incrementally enhancing device conductivity, reminiscent of PPF. Device conductivity eventually reaches a saturation point (the fatigue

zone) due to the electric field driving an increased number of oxygen vacancies towards connected conductive pathways, decreasing vacancies in original clusters. Thus, the available oxygen vacancy count drops, causing a reduction in the rate of conductivity increase. This dynamic is intrinsically tied to the external field, “E,” illustrated in Figure 5, independent of the HfZrO layer’s intrinsic ferroelectric characteristics “P,” and does not dictate current behavior during pulse intervals, aligning with the mechanisms described without contradiction. This coexistent process could lead to PPF-like current increases within the HfZrO layer.

In assessing the effect of pulse characteristics on current amplification, we examined three principal factors: amplitude, interval, and pulse duration. This examination, delineated in Figure 6, seeks to elucidate the influence of pulse dynamics on current enhancement. Here, the Increment Ratio (IR) is mathematically represented as:

$$IR = (I_n - I_{n-1})/I_1 \tag{2}$$

where I_n symbolizes the current in the n th one. By varying one of these pulse characteristics while maintaining the others constant, we delve into the role each plays in modulating the current increment ratio. Figure 6 demonstrates that augmenting pulse strength—through enhanced pulse width, reduced intervals, or increased amplitude—positively impacts the IR. Nonetheless, with further intensification of pulse strength, the IR’s progression plateaus, indicating a trend towards stabilization. This phenomenon suggests that while stronger pulses notably decrease the memristor’s resistance, leading to amplified currents, there exists a persistent “fatigue” effect, akin to the brain’s adaptive response to recurrent stimuli, constrained by the dynamic oxygen vacancy mechanism within a finite pulse duration spectrum.

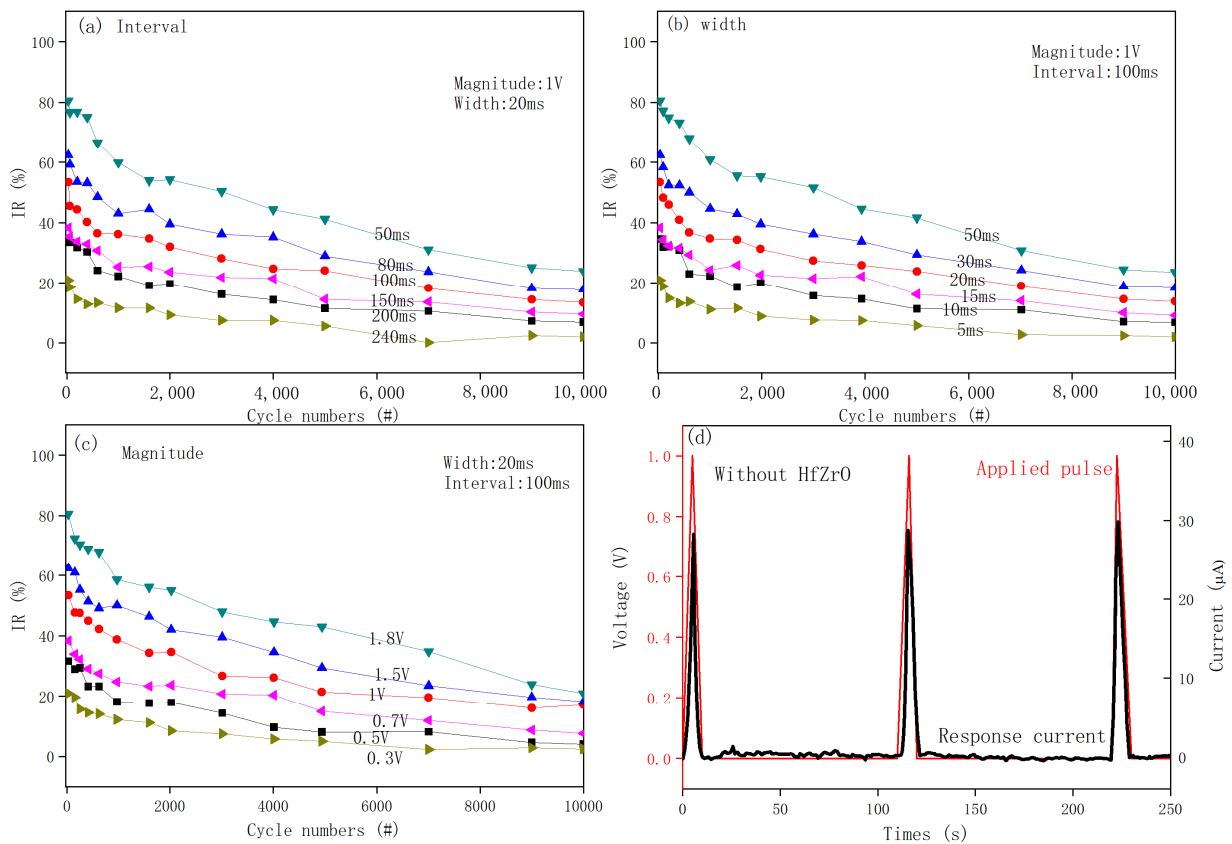


Figure 6. Relationship between the Increment Ratio (IR) with the number of cycles under (a) increasing intervals, (b) increasing widths, and (c) increasing amplitudes. (d) Response current (black) of a pure ZnO device of the same thickness (without HfZrO layer) for comparison. The pulse is present in red. The current ceases during the pulse off periods.

Variability in the interval between consecutive pulses influences the facilitation effect, with a pronounced decrement observed as intervals extend, as depicted in Figure 6. At extended pulse intervals, the increment in device conductivity (mirroring PPF effects) commences from its basal conductive state, with elongated intervals diminishing the increment pace. Subsequent analyses are omitted, as device conductance shows negligible facilitation beyond certain interval lengths, suggesting that conductive pathways initially established by a series of pulses may disintegrate before the arrival of subsequent pulses. This reaggregation of oxygen vacancies (or ions) back to their initial positions within ZnO or cluster formations in HfZrO has been previously documented, shedding light on the nuanced interplay between pulse parameters and conductive behavior in memristive devices.

The architecture of the device explored in our research, comprising ZnO and HfZrO layers, marks a departure from the single-layered device configurations previously identified for demonstrating PPF phenomena. Notably, our device showcases a sustained post-synaptic current beyond the cessation of input voltage pulses, exhibiting a more distinct PPF effect that escalates with successive pulse trains. This underscores the critical influence of the highly oxygen-deficient HfZrO layer on the device's performance. Comparative analysis presented in Figure 6d with pure ZnO devices reveals a cessation in current flow upon pulse discontinuation, aligning with earlier findings. The diverse properties manifested by Hf-based oxides, including HfO₂ and HfZrO, at varying oxygen levels—spanning p-type conductance, fluorescence, ferroelectricity, to intrinsic d0 magnetism—are largely ascribed to their highly oxygen-deficient conditions and/or dopant presence, which may induce lattice distortions fostering ferroelectricity. Despite the elusive ferroelectric mechanism underlying HfZrO, its proven compatibility with semiconductor processes harbors significant potential. Our observations of enduring post-synaptic currents hint at the promising avenue for ferroelectricity-driven artificial synaptic research opened by the oxygen-deficient state of HfZrO.

In addition, Electroforming, a critical one-time electrical “formatting” process, sets the memristor's resistive state to a reusable initial setting prior to its first use. In our ZnO/HfZrO bilayer structure, the combination of ZnO's excellent carrier properties and HfZrO's spontaneous polarization electric field most likely initiates electroforming behavior during the annealing and forming processes. This improves resistive regulation convenience, which is critical for replicating complex biological synaptic dynamics. Furthermore, our device operates without compliance current, ensuring stability in the absence of external current limitation during resistive switching. This simplicity improves device reliability, which is especially useful for long-term or high-frequency tasks, paving the way for its use in high-frequency signal processing and long-term learning memory mechanisms. Applying a series of 1 V pulse voltages allows for high-frequency, low-power operation, which is similar to the key characteristics of biological synapses. The bilayer device's performance in these areas demonstrates its potential and distinct advantages in simulating biological behaviors.

4. Conclusions

In conclusion, it reveals that ZnO/HfZrO-based memristors demonstrate adaptation and fatigue behaviors under sequential electrical pulse stimulations, mirroring the memory mechanisms observed in biological entities. Despite the initial increase in conductivity prompted by ongoing pulse stimulation, the extent of this enhancement shows a progressive decline. Notably, the study observed a temperature-dependent relaxation phenomenon in current retention. The pivotal role of oxygen vacancies (ions) maneuvering in response to external pulsing and inherent polarization fields marks a significant pathway in the STM to LTM memory evolution. Reinforced through methodical stimulation training, STM undergoes amplification, transitioning into LTM, a process closely tied to the structural transition from a state of flux to one of consolidation facilitated by the sequence of pulses. While continuous efforts are underway to refine and broaden synaptic emulation, the

documented habituation behaviors underscore the memristor's potential in mimicking biological neuronal activities.

Author Contributions: Validation, J.L.; Formal analysis, Z.W.; Investigation, Z.X., K.W., R.L., L.W. and F.Y.; Data curation, H.J.; Writing—original draft, M.S.; Funding acquisition, R.J. All authors have read and agreed to the published version of the manuscript.

Funding: This research was funded by the Natural Science Foundation of Ningbo Municipality (2023J007), the Natural Sciences Fund of Zhejiang Province (LDT23F05015F05). This work was also supported by the Opening Project of Key Laboratory of Microelectronic Devices & Integrated Technology Institute of Microelectronics, Chinese Academy of Sciences.

Data Availability Statement: The data presented in this study are available in this article.

Conflicts of Interest: The authors declare no conflict of interest.

References

1. Jaeger, H. Exploring the landscapes of “computing”: Digital, neuromorphic, unconventional—And beyond. *arXiv Prepr.* **2020**, arXiv:2011.12013.
2. Wan, Q.; Sharbati, M.T.; Erickson, J.R.; Du, Y.; Xiong, F. Emerging artificial synaptic devices for neuromorphic computing. *Adv. Mater. Technol.* **2019**, *4*, 1900037. [[CrossRef](#)]
3. Caravelli, F.; Carbajal, J.P. Memristors for the curious outsiders. *Technologies* **2018**, *6*, 118. [[CrossRef](#)]
4. Jeong, D.S.; Kim, K.M.; Kim, S.; Choi, B.J.; Hwang, C.S. Memristors for energy-efficient new computing paradigms. *Adv. Electron. Mater.* **2016**, *2*, 1600090. [[CrossRef](#)]
5. Radamson, H.H.; Zhu, H.; Wu, Z.; He, X.; Lin, H.; Liu, J.; Xiang, J.; Kong, Z.; Xiong, W.; Li, J. State of the art and future perspectives in advanced CMOS technology. *Nanomaterials* **2020**, *10*, 1555. [[CrossRef](#)] [[PubMed](#)]
6. Feng, P.; Xu, W.; Yang, Y.; Wan, X.; Shi, Y.; Wan, Q.; Zhao, J.; Cui, Z. Printed neuromorphic devices based on printed carbon nanotube thin-film transistors. *Adv. Funct. Mater.* **2017**, *27*, 1604447. [[CrossRef](#)]
7. Schulz, P.E.; Cook, E.P.; Johnston, D. Changes in paired-pulse facilitation suggest presynaptic involvement in long-term potentiation. *J. Neurosci.* **1994**, *14*, 5325–5337. [[CrossRef](#)]
8. Li, H.; Geng, S.; Liu, T.; Cao, M.; Su, J. Synaptic and Gradual Conductance Switching Behaviors in CeO₂/Nb–SrTiO₃ Heterojunction Memristors for Electrocardiogram Signal Recognition. *ACS Appl. Mater. Interfaces* **2023**, *15*, 5456–5465. [[CrossRef](#)]
9. Niu, J.; Fang, Z.; Liu, G.; Zhao, Z.; Yan, X. Multilevel state ferroelectric La: HfO₂-based memristors and their implementations in associative learning circuit and face recognition. *Sci. China Mater.* **2023**, *66*, 1148–1156. [[CrossRef](#)]
10. Qi, M.; Fu, T.; Yang, H.; Tao, Y.; Li, C.; Xiu, X. Reliable analog resistive switching behaviors achieved using memristive devices in AlO_x/HfO_x bilayer structure for neuromorphic systems. *Semicond. Sci. Technol.* **2022**, *37*, 035018. [[CrossRef](#)]
11. Ismail, M.; Rasheed, M.; Mahata, C.; Kang, M.; Kim, S. Mimicking biological synapses with a-HfSiO_x-based memristor: Implications for artificial intelligence and memory applications. *Nano Converge.* **2023**, *10*, 33. [[CrossRef](#)]
12. Ryu, H.; Kim, S. Self-Rectifying Resistive Switching and Short-Term Memory Characteristics in Pt/HfO₂/TaO_x/TiN Artificial Synaptic Device. *Nanomaterials* **2020**, *10*, 2159. [[CrossRef](#)]
13. Khot, A.C.; Dongale, T.D.; Nirmal, K.A.; Deepthi, J.K.; Sutar, S.S.; Kim, T.G. 2D Ti₃C₂T_x MXene-derived self-assembled 3D TiO₂nanoflowers for nonvolatile memory and synaptic learning applications. *J. Mater. Sci. Technol.* **2023**, *150*, 1–10. [[CrossRef](#)]
14. Cao, G.; Meng, P.; Chen, J.; Liu, H.; Bian, R.; Zhu, C.; Liu, F.; Liu, Z. 2D material based synaptic devices for neuromorphic computing. *Adv. Funct. Mater.* **2021**, *31*, 2005443. [[CrossRef](#)]
15. Zhao, P.; Ji, R.; Lao, J.; Jiang, C.; Tian, B.; Luo, C.; Lin, H.; Peng, H.; Duan, C.-G. Multifunctional two-terminal optoelectronic synapse based on zinc oxide/Poly (3-hexylthiophene) heterojunction for neuromorphic computing. *ACS Appl. Polym. Mater.* **2022**, *4*, 5688–5695. [[CrossRef](#)]
16. Song, W.; Yu, H.; Li, X.; Fang, R.; Zhu, W.; Zhang, L. Electric-Controlled Resistive Switching and Different Synaptic Behaviors in p⁺-Si/n-ZnO Heterojunction Memristor. *IEEE Trans. Electron Devices* **2023**, *70*, 1648–1652. [[CrossRef](#)]
17. Li, W.; Fan, Z.; Huang, Q.; Rao, J.; Cui, B.; Chen, Z.; Lin, Z.; Yan, X.; Tian, G.; Tao, R. Polarization-dominated internal timing mechanism in a ferroelectric second-order memristor. *Phys. Rev. Appl.* **2023**, *19*, 014054. [[CrossRef](#)]
18. Xiao, C.; Xu, B.; Si, J.; Di, Z.; Zhao, L.; Liu, R.; Lv, Q.; Wang, L.; Zhang, L. Wide waveband light detection and storage device for visual memory. *Phys. Status Solidi (A)* **2022**, *219*, 2100881. [[CrossRef](#)]
19. Hong, Q.; Yan, R.; Wang, C.; Sun, J. Memristive circuit implementation of biological nonassociative learning mechanism and its applications. *IEEE Trans. Biomed. Circuits Syst.* **2020**, *14*, 1036–1050. [[CrossRef](#)] [[PubMed](#)]
20. Li, Y.; Su, K.; Chen, H.; Zou, X.; Wang, C.; Man, H.; Liu, K.; Xi, X.; Li, T. Research progress of neural synapses based on memristors. *Electronics* **2023**, *12*, 3298. [[CrossRef](#)]
21. Wang, Z.; Wang, L.; Nagai, M.; Xie, L.; Yi, M.; Huang, W. Nanoionics-enabled memristive devices: Strategies and materials for neuromorphic applications. *Adv. Electron. Mater.* **2017**, *3*, 1600510. [[CrossRef](#)]

22. Cao, Z.; Sun, B.; Zhou, G.; Mao, S.S.; Zhu, S.H.; Zhang, J.; Ke, C.; Zhao, Y.; Shao, J. Memristor-based neural networks: A bridge from device to artificial intelligence. *Nanoscale Horiz.* **2023**, *8*, 716–745. [[CrossRef](#)]
23. Cowan, N. Short-term memory based on activated long-term memory: A review in response to Norris (2017). *Psychol. Bull.* **2019**, *145*, 822–847. [[CrossRef](#)]
24. Kim, T.; Jeon, S. Pulse switching study on the HfZrO ferroelectric films with high pressure annealing. *IEEE Trans. Electron Devices* **2018**, *65*, 1771–1773. [[CrossRef](#)]
25. Yadav, M.; Kashir, A.; Oh, S.; Nikam, R.D.; Kim, H.; Jang, H.; Hwang, H. High polarization and wake-up free ferroelectric characteristics in ultrathin Hf_{0.5}Zr_{0.5}O₂ devices by control of oxygen-deficient layer. *Nanotechnology* **2021**, *33*, 085206. [[CrossRef](#)] [[PubMed](#)]
26. Yun, S.; Mahata, C.; Kim, M.-H.; Kim, S. Artificial synapse characteristics of a ZnO-based memristor with a short-term memory effect. *Appl. Surf. Sci.* **2022**, *579*, 152164. [[CrossRef](#)]
27. Pereira, M.; Deuermeier, J.; Freitas, P.; Barquinha, P.; Zhang, W.; Martins, R.; Fortunato, E.; Kiazadeh, A.; Hiroya, I. Tailoring the synaptic properties of a-IGZO memristors for artificial deep neural networks. *APL Mater.* **2022**, *10*, 011113. [[CrossRef](#)]
28. Hu, M.; Chen, Y.; Yang, J.J.; Wang, Y.; Li, H.H. A compact memristor-based dynamic synapse for spiking neural networks. *IEEE Trans. Comput.-Aided Des. Integr. Circuits Syst.* **2016**, *36*, 1353–1366. [[CrossRef](#)]
29. Min, D.-H.; Ryu, T.-H.; Yoon, S.-J.; Moon, S.-E.; Yoon, S.-M. Improvements in the synaptic operations of ferroelectric field-effect transistors using Hf_{0.5}Zr_{0.5}O₂ thin films controlled by oxygen partial pressures during the sputtering deposition process. *J. Mater. Chem. C* **2020**, *8*, 7120–7131. [[CrossRef](#)]
30. Liu, C.; Shen, X.; Fan, S.; Xu, T.; Zhang, J.; Su, J. Synaptic Characteristics and Neuromorphic Computing Enabled by Oxygen Vacancy Migration Based on Porous In₂O₃ Electrolyte-Gated Transistors. *ACS Appl. Electron. Mater.* **2023**, *5*, 4657–4666. [[CrossRef](#)]
31. Mahata, C.; So, H.; Kim, S.; Kim, S.; Cho, S. Analog Memory and Synaptic Plasticity in an InGaZnO-Based Memristor by Modifying Intrinsic Oxygen Vacancies. *Materials* **2023**, *16*, 7510. [[CrossRef](#)] [[PubMed](#)]
32. Tian, H.; Mi, W.; Zhao, H.; Mohammad, M.A.; Yang, Y.; Chiu, P.-W.; Ren, T.-L. A novel artificial synapse with dual modes using bilayer graphene as the bottom electrode. *Nanoscale* **2017**, *9*, 9275–9283. [[CrossRef](#)] [[PubMed](#)]
33. Nayagam, D.A.; Williams, R.A.; Allen, P.J.; Shivdasani, M.N.; Luu, C.D.; Salinas-LaRosa, C.M.; Finch, S.; Ayton, L.N.; Saunders, A.L.; McPhedran, M. Chronic electrical stimulation with a suprachoroidal retinal prosthesis: A preclinical safety and efficacy study. *PLoS ONE* **2014**, *9*, e97182. [[CrossRef](#)] [[PubMed](#)]
34. Cowan, N. The magical number 4 in short-term memory: A reconsideration of mental storage capacity. *Behav. Brain Sci.* **2001**, *24*, 87–114. [[CrossRef](#)]
35. Tripathy, S.P.; Ögmen, H. Sensory memory is allocated exclusively to the current event-segment. *Front. Psychol.* **2018**, *9*, 1435. [[CrossRef](#)] [[PubMed](#)]
36. Wood, R.; Baxter, P.; Belpaeme, T. A review of long-term memory in natural and synthetic systems. *Adapt. Behav.* **2012**, *20*, 81–103. [[CrossRef](#)]
37. Ielmini, D.; Wang, Z.; Liu, Y. Brain-inspired computing via memory device physics. *APL Mater.* **2021**, *9*, 050702. [[CrossRef](#)]
38. Ma, F.; Zhu, Y.; Xu, Z.; Liu, Y.; Zheng, X.; Ju, S.; Li, Q.; Ni, Z.; Hu, H.; Chai, Y. Optoelectronic perovskite synapses for neuromorphic computing. *Adv. Funct. Mater.* **2020**, *30*, 1908901. [[CrossRef](#)]
39. Yamada, C.; Itaguchi, Y.; Fukuzawa, K. Effects of the amount of practice and time interval between practice sessions on the retention of internal models. *PLoS ONE* **2019**, *14*, e0215331. [[CrossRef](#)]
40. Sokolov, A.S.; Ali, M.; Riaz, R.; Abbas, Y.; Ko, M.J.; Choi, C. Silver-adapted diffusive memristor based on organic nitrogen-doped graphene oxide quantum dots (N-GOQDs) for artificial biosynapse applications. *Adv. Funct. Mater.* **2019**, *29*, 1807504. [[CrossRef](#)]
41. Kim, S.; Choi, S.; Lu, W. Comprehensive physical model of dynamic resistive switching in an oxide memristor. *ACS Nano* **2014**, *8*, 2369–2376. [[CrossRef](#)]
42. Du, C.; Ma, W.; Chang, T.; Sheridan, P.; Lu, W.D. Biorealistic implementation of synaptic functions with oxide memristors through internal ionic dynamics. *Adv. Funct. Mater.* **2015**, *25*, 4290–4299. [[CrossRef](#)]
43. Min, Y.; Akbulut, M.; Kristiansen, K.; Golan, Y.; Israelachvili, J. The role of interparticle and external forces in nanoparticle assembly. *Nat. Mater.* **2008**, *7*, 527–538. [[CrossRef](#)]
44. Hsieh, P.-T.; Chen, Y.-C.; Kao, K.-S.; Wang, C.-M. Luminescence mechanism of ZnO thin film investigated by XPS measurement. *Appl. Phys. A* **2008**, *90*, 317–321. [[CrossRef](#)]
45. Chen, M.; Wang, X.; Yu, Y.; Pei, Z.; Bai, X.; Sun, C.; Huang, R.; Wen, L. X-ray photoelectron spectroscopy and auger electron spectroscopy studies of Al-doped ZnO films. *Appl. Surf. Sci.* **2000**, *158*, 134–140. [[CrossRef](#)]
46. Wang, Z.Q.; Xu, H.Y.; Li, X.H.; Yu, H.; Liu, Y.C.; Zhu, X.J. Synaptic learning and memory functions achieved using oxygen ion migration/diffusion in an amorphous InGaZnO memristor. *Adv. Funct. Mater.* **2012**, *22*, 2759–2765. [[CrossRef](#)]
47. Li, Y.; Liang, R.; Wang, J.; Zhang, Y.; Tian, H.; Liu, H.; Li, S.; Mao, W.; Pang, Y.; Li, Y. A ferroelectric thin film transistor based on annealing-free HfZrO film. *IEEE J. Electron Devices Soc.* **2017**, *5*, 378–383. [[CrossRef](#)]
48. Yang, Y.; Lu, W. Nanoscale resistive switching devices: Mechanisms and modeling. *Nanoscale* **2013**, *5*, 10076–10092. [[CrossRef](#)] [[PubMed](#)]
49. Liu, L.; Mei, Z.; Tang, A.; Azarov, A.; Kuznetsov, A.; Xue, Q.-K.; Du, X. Oxygen vacancies: The origin of n-type conductivity in ZnO. *PhRvB* **2016**, *93*, 235305. [[CrossRef](#)]

50. Yang, R.; Wang, F.; Lu, J.; Lu, Y.; Lu, B.; Li, S.; Ye, Z. ZnO with p-Type Doping: Recent Approaches and Applications. *ACS Appl. Electron. Mater.* **2023**, *5*, 4014–4034. [[CrossRef](#)]
51. Jiang, R.; Du, X.; Han, Z.; Sun, W. Investigation of chemical distribution in the oxide bulk layer in Ti/HfO₂/Pt memory devices using X-ray photoelectron spectroscopy. *Appl. Phys. Lett.* **2015**, *106*, 173509. [[CrossRef](#)]
52. Wang, Z.; Joshi, S.; Savel'ev, S.E.; Jiang, H.; Midya, R.; Lin, P.; Hu, M.; Ge, N.; Strachan, J.P.; Li, Z. Memristors with diffusive dynamics as synaptic emulators for neuromorphic computing. *Nat. Mater.* **2017**, *16*, 101–108. [[CrossRef](#)] [[PubMed](#)]

Disclaimer/Publisher's Note: The statements, opinions and data contained in all publications are solely those of the individual author(s) and contributor(s) and not of MDPI and/or the editor(s). MDPI and/or the editor(s) disclaim responsibility for any injury to people or property resulting from any ideas, methods, instructions or products referred to in the content.